PHOTONICS Research

Ultrastable Gd^{3+} doped $CsPbCl_{1.5}Br_{1.5}$ nanocrystals blue glass for regulated and low thresholds amplified spontaneous emission

Qingyun He,[1] Enrou Mei,[1] Ze Wang,[1] Xiaojuan Liang,[1,2] Suqin Chen,[1,3] and Weidong Xiang[1,*]

[1]College of Chemistry and Materials Engineering, Wenzhou University, Wenzhou 325035, China
[2]e-mail: lxj6126@126.com
[3]e-mail: csqcsq125@wzu.edu.cn
*Corresponding author: xiangweidong001@126.com

Received 13 May 2021; revised 30 June 2021; accepted 17 July 2021; posted 20 July 2021 (Doc. ID 431387); published 9 September 2021

Here, Gd-doped $CsPbCl_{1.5}Br_{1.5}$ nanocrystals (NCs) in borosilicate glass matrix (B_2O_3–SiO_2–ZnO) were prepared by melting quenching and *in-situ* crystallization. The optical performance of $CsPbCl_{1.5}Br_{1.5}$ NCs glasses under different heat-treatment temperatures and the content of Gd^{3+} were analyzed in detail. After $CsPbCl_{1.5}Br_{1.5}$ NCs glass is doped with Gd^{3+} ions, the photoluminescence intensity increases and the synthesized Gd-doped $CsPbCl_{1.5}Br_{1.5}$ NCs glasses have excellent water stability and thermal cycling performance. In addition, the influence of Gd-doped concentrations and heat-treatment temperatures on the amplified spontaneous emission (ASE) thresholds of $CsPbCl_{1.5}Br_{1.5}$ NCs glasses was studied, and the Gd-doped $CsPbCl_{1.5}Br_{1.5}$ NCs glasses achieve controllable ASE thresholds at room temperature. The ASE threshold can be as low as 0.39 mJ/cm^2. This work offers a neoteric reference for the research in the application of metal ion-doped perovskite NCs and a new idea for the realization of controllable and low ASE thresholds on perovskite NCs.

https://doi.org/10.1364/PRJ.431387

1. INTRODUCTION

Metal halide perovskites (i.e., $CsPbX_3$, X = Cl, Br, and I) materials have broad application prospects in the fields of high-definition displays, solar cells, abyss communications, and optoelectronic devices [1–7]. As a direct bandgap semiconductor, perovskite has the advantages of the adjustable bandgap, high optical gain, large absorption coefficient, high quantum yield, and low defect state density [8–13]. It has become an ideal material for designing low-threshold, color laser devices [14–19]. Despite such bright prospects, the rapid luminescence quenching and poor hydrothermal stability of perovskite nanocrystals (NCs) severely impede their practical applications in the laser field [20].

In order to optimize the stability of perovskite NCs, several different means have been employed [21–25]. Protesescu *et al.* reported $FAPbBr_3$ NCs with a strongly improved chemical stability during purification processes and good amplified spontaneous emission (ASE) properties [26]. Krieg *et al.* synthesized $CsPbBr_3$ NCs with a low ASE threshold capped with zwitterionic long-chain molecules, which further improved the long-term stability of NCs [27]. Yan *et al.* recently modified the ligands by replacing the oleic acid (OA) ligands with 2-hexyldecanoic acid (DA) to improve the stability of $CsPbBr_3$ NCs, and DA functionalized NCs showed a lower ASE threshold than OA affected NCs [28]. Although ligand modification, surface modification, and formation of core layer structure can effectively stabilize perovskite NCs [29–33], there is still much room for improvement in stabilizing $CsPbX_3$ NCs. Alternatively, since inorganic glass can protect $CsPbX_3$ NCs from the external environment, embedding $CsPbX_3$ NCs in glass has acted as one of the effective methods to improve the stability of perovskite NCs [34]. It is important that the perovskite NCs embedded in the glass not only exhibit ultrastable performance, but also have a low ASE threshold.

Although researchers have recently worked hard to adjust the ASE thresholds of perovskite NCs by adding organic molecular additives [35], zinc oxide nanoparticles [36], silver nanoparticles, [37], and changing the morphology and roughness of the sample [38], particle size also plays a vital role in regulating the ASE thresholds [39]. Fortunately, the size of perovskite NCs can be adjusted by controlling the doping of metal ions and the heat treatment temperatures. Furthermore, there are few reports linking the doping of metal ions and heat treatment conditions with the ASE thresholds of perovskite NCs at the same time. Based on the above, it is necessary to prepare a series of Gd-doped $CsPbCl_{1.5}Br_{1.5}$ NCs glasses to study the effect of Gd^{3+} concentrations and heat treatment temperatures on the ASE thresholds of perovskite NCs. Excitingly, the prepared Gd-doped $CsPbCl_{1.5}Br_{1.5}$ NCs glasses can exhibit ASE

characteristics, and it is found that doping metal ions and heat treatment temperatures have a regulatory function on the ASE thresholds of Gd-doped $CsPbCl_{1.5}Br_{1.5}$ NCs glasses.

In this work, a series of Gd-doped $CsPbCl_{1.5}Br_{1.5}$ NCs emitting blue light were successfully synthesized in borosilicate glass by the traditional melting quenching method. The adjustment on the bandgap and wavelength of Gd-doped $CsPbCl_{1.5}Br_{1.5}$ NCs glasses can be achieved by changing the doping concentration and heat treatment temperature. Moreover, the prepared Gd-doped $CsPbCl_{1.5}Br_{1.5}$ NCs glass possesses good optical performance and excellent hydrothermal stability. Finally, under 800 nm fs pulsed laser at room temperature, not at low temperature, Gd-doped $CsPbCl_{1.5}Br_{1.5}$ NCs glasses can be used in the laser field, and the ASE threshold of Gd-doped $CsPbCl_{1.5}Br_{1.5}$ NCs glass is as low as 0.39 mJ/cm^2.

2. EXPERIMENT

A. Materials

Cesium carbonate (Cs_2CO_3, 99.9%), lead bromide ($PbBr_2$, 99%), lead chloride ($PbCl_2$, 98%), gadolinium fluoride (GdF_3, 99.9%), sodium chloride (NaCl, 99.5%), sodium bromide (NaBr, 99.9%), silicon dioxide (SiO_2, 99%), boron oxide (B_2O_3, 99.9%), and zinc oxide (ZnO, 99%) were bought from Aladdin. All chemicals were used without further treatment.

B. Synthesis of Gd-Doped $CsPbCl_{1.5}Br_{1.5}$ NCs Glasses

ZnO (molar percentage: 14.27%), B_2O_3 (32.80%), and SiO_2 (28.27%) were first weighed as the glass matrix in the preparation of Gd-doped $CsPbCl_{1.5}Br_{1.5}$ NCs glasses. The three ingredients were mixed and milled uniformly in the mortar, and then NaBr (5.58%), NaCl (5.58%), $PbBr_2$ (2.48%), $PbCl_2$ (2.48%), and Cs_2CO_3 (8.54%) were put into the alumina crucible. The crucible was put in the heating furnace and was heated to 1200°C for 10 min to ensure that everything melts. Then the crucible was taken out and poured into a grinding tool preheated to 400°C. After the glass was slightly shaped, it was quickly put in an oven at 400°C and heated for 3 h and cooled to room temperature naturally. This heat preservation process is a necessary process, called annealing. It is designed to eliminate the internal stress of the $CsPbCl_{1.5}Br_{1.5}$ NCs precursor glass and prevent the newly formed glass melt from breaking due to a sudden drop in temperature. A series of Gd-doped $CsPbCl_{1.5}Br_{1.5}$ NCs glasses were obtained by regulating the concentration of GdF_3 (GdF_3 concentration of 0%, 0.5%, 1%, 3%, respectively marked as S1, S2, S3, and S4).

C. Characterization

Using Bruker D8 Advance measurement, the phase structure of the samples was characterized by X-ray diffraction (XRD). It is pointed out that the Cu K_α radiation of Bruker D8 Advance measurements was running in the boundary of 10°–60° (2θ) at the velocity of 0.02° per second (the current as 40 mA and the voltage as 40 kV). The ultraviolet–visible (UV-vis) spectra were surveyed by a PerkinElmer 750 UV-vis spectrometer, and the recording scope was 400–600 nm. The JEOL JEm-2100F transmission electron microscope (TEM) was used to observe the microstructure of perovskite NCs. The distribution of elements was tested with TEM-assisted energy dispersive spectrometer (EDS). The temperature-dependent photoluminescence (PL) spectra were measured with THMS 600. Under the excitation of the commercially available Ti:sapphire regenerative amplifier (800 nm, 35 fs, 1 kHz) at room temperature, the ASE of perovskite NCs glasses has been actively studied. A cylindrical lens with a focal length of 10 cm was used to focus the laser beam onto the surface of the sample. Adjustable slits could be used to precisely control the fringe length of the light spot. The ASE was detected by a fiber optic spectrometer (Marine Optics) with a spectral resolution of 1 nm. The fluorescence and absorption measurements are all under the same excitation wavelength of 365 nm.

3. RESULTS AND DISCUSSION

The network structure of borosilicate glass is silicon oxide tetrahedron, which is mainly composed of bridged and non-bridged oxygen bonds. In the precursor borosilicate glass, Cs^+, Pb^{2+}, Gd^{3+}, F^-, Cl^-, and Br^- ions are distributed in the borosilicate glass. Once external conditions give these ions enough energy to reach the formation energy of Gd-doped $CsPbCl_{1.5}Br_{1.5}$ NCs, Cs^+, Pb^{2+}, Cl^-, and Br^- ions will migrate to the network voids to nucleate and grow. However, due to the inconsistent size of the network voids, the size of the formed perovskite NCs is also not uniform [40]. To explore the optimal Gd^{3+} concentration in $CsPbCl_{1.5}Br_{1.5}$ NCs glasses, a series of Gd-doped $CsPbCl_{1.5}Br_{1.5}$ NCs glasses were synthesized, and they all emitted bright blue light under UV light [Fig. 1(c)]. Then, the PL of Gd-doped $CsPbCl_{1.5}Br_{1.5}$ NCs glasses was tested. As shown in Fig. 1(a), a certain amount of Gd^{3+} doping promotes the increase of the PL intensity of $CsPbCl_{1.5}Br_{1.5}$ NCs glasses, but excessive Gd^{3+} doping quenches the PL intensity of $CsPbCl_{1.5}Br_{1.5}$ NCs glasses. It can be concluded that the best Gd^{3+} doping in $CsPbCl_{1.5}Br_{1.5}$ NCs glasses is found to be 1% (S3). The quantum efficiencies of S1–S4 are 5.1%, 10.3%, 12%, and 2%, respectively. Gd^{3+} doping improves the optical performance of $CsPbCl_{1.5}Br_{1.5}$ NCs glasses because Gd^{3+} ions reduce defects, which enhances radiative recombination and reduces non-radiative recombination paths [41]. As for F^- ion, F^- ion promotes a part of Gd^{3+} doping into $CsPbCl_{1.5}Br_{1.5}$ NCs glasses by fracturing the silicon–oxygen bonds and generating non-bridging oxygen bonds [42]. In addition, the PL emission peak position has a slight blueshift as the Gd^{3+} concentration increases, which may be because part of Gd^{3+} replaces Pb^{2+} caused by the reduction of the particle size. Figure 1(b) shows that as the Gd^{3+} concentration increases, the bandgap energy increases, which is caused by more Gd^{3+} entering the lattice leading to the shrinkage of the perovskite NCs lattice. Since perovskite NCs are direct interband transitions, the formula can be used to calculate the optical bandgap E_g of Gd-doped $CsPbCl_{1.5}Br_{1.5}$ NCs glasses as follows [43]:

$$(\alpha h\nu)^2 = A(h\nu - E_g),$$

where A is the parameter concerning the effective mass of the valence and conduction bands, h is Planck's constant, α is the absorption coefficient, and ν represents the optical frequency.

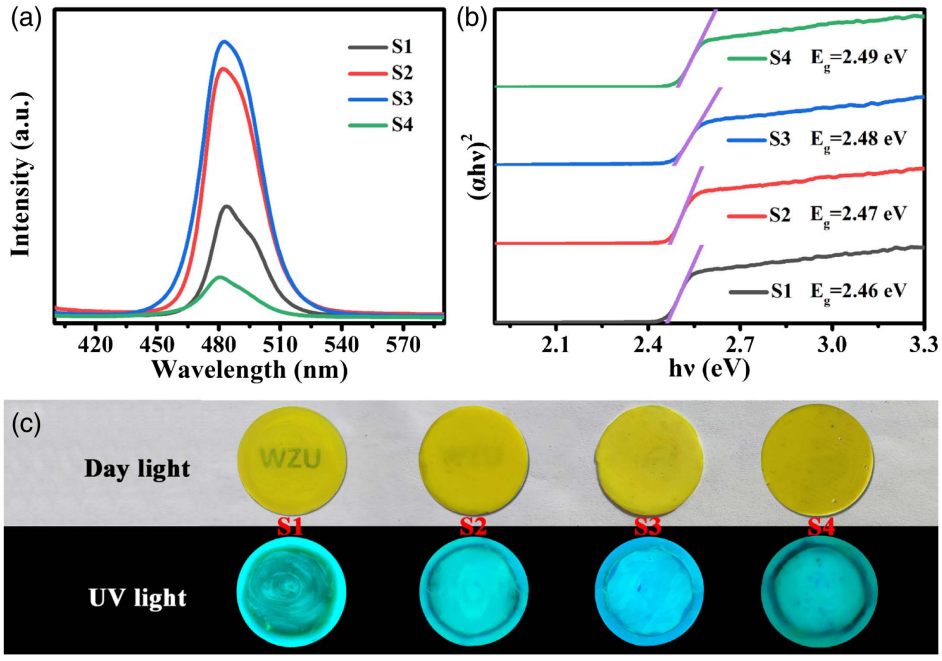

Fig. 1. (a) PL spectra. (b) Spectra plotted as $(\alpha h\nu)^2 - h\nu$ of Gd-doped $CsPbCl_{1.5}Br_{1.5}$ NCs glasses. (c) Photos of a series of Gd-doped $CsPbCl_{1.5}Br_{1.5}$ NCs glasses (S1–S4) (from left to light) in daylight and ultraviolet (UV) light.

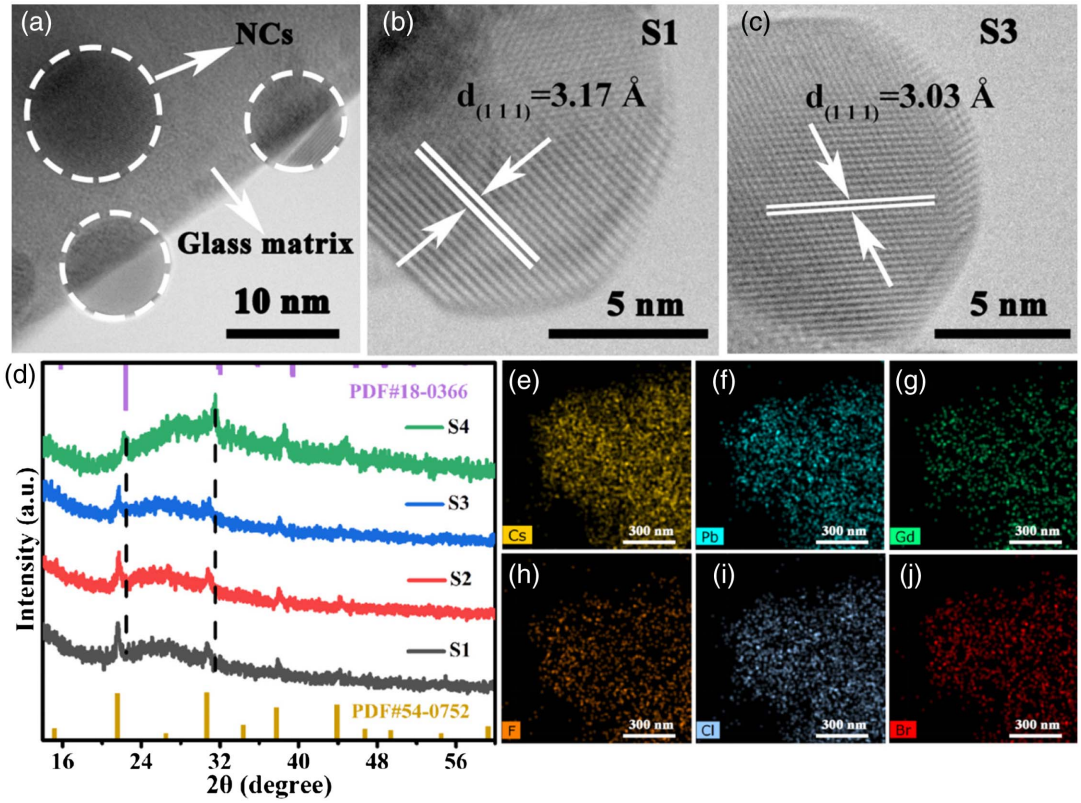

Fig. 2. (a) TEM image of Gd-doped $CsPbCl_{1.5}Br_{1.5}$ NCs glass. (b) HRTEM image of $CsPbCl_{1.5}Br_{1.5}$ NCs glass (S1). (c) HRTEM image of Gd-doped $CsPbCl_{1.5}Br_{1.5}$ NCs glass (S3). (d) XRD patterns of Gd-doped $CsPbCl_{1.5}Br_{1.5}$ NCs glasses. (e)–(j) EDS elemental mappings of Gd-doped $CsPbCl_{1.5}Br_{1.5}$ NCs glass.

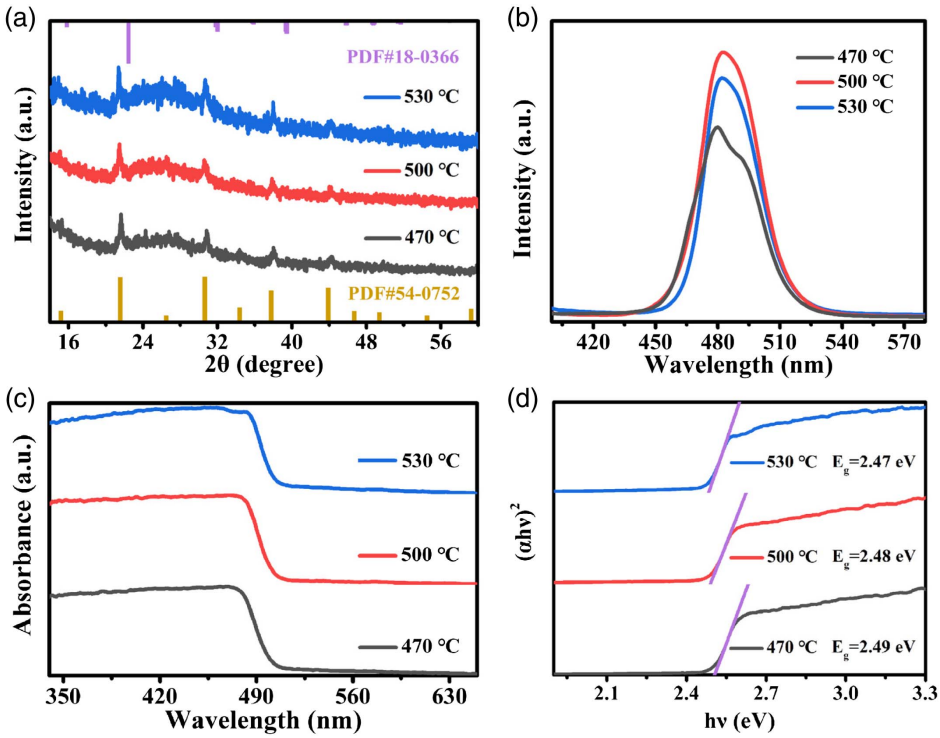

Fig. 3. (a) XRD patterns, (b) PL spectra, (c) UV-vis absorption spectra. (d) Spectra plotted as $(\alpha h\nu)^2$ – $h\nu$ of Gd-doped $CsPbCl_{1.5}Br_{1.5}$ NCs glasses (470°C–530°C).

Next, the phase structure and microstructure of Gd-doped $CsPbCl_{1.5}Br_{1.5}$ NCs glasses were analyzed. It can be seen from Fig. 2(d) that the diffraction peaks are located between the standard diffraction cards (PDF#54–0752 is the standard diffraction card of cubic $CsPbBr_3$ and PDF#18–0366 is the standard diffraction card of cubic $CsPbCl_3$), demonstrating that the $CsPbCl_{1.5}Br_{1.5}$ NCs were successfully precipitated in the borosilicate glass matrix. In addition, it can also be seen that the diffraction peak intensities of doped and undoped $CsPbCl_{1.5}Br_{1.5}$ NCs glasses are quite strong, indicating that the crystallinity of the perovskite NCs in S1–S4 is good. It needs to be emphasized that, with the increase of Gd^{3+} content, the XRD peaks of $CsPbCl_{1.5}Br_{1.5}$ NCs glasses move slightly to a larger angle. This shift is attributed to the contraction of the crystal lattice, which is due to the partial replacement of Pb^{2+} with a larger radius by Gd^{3+} with a

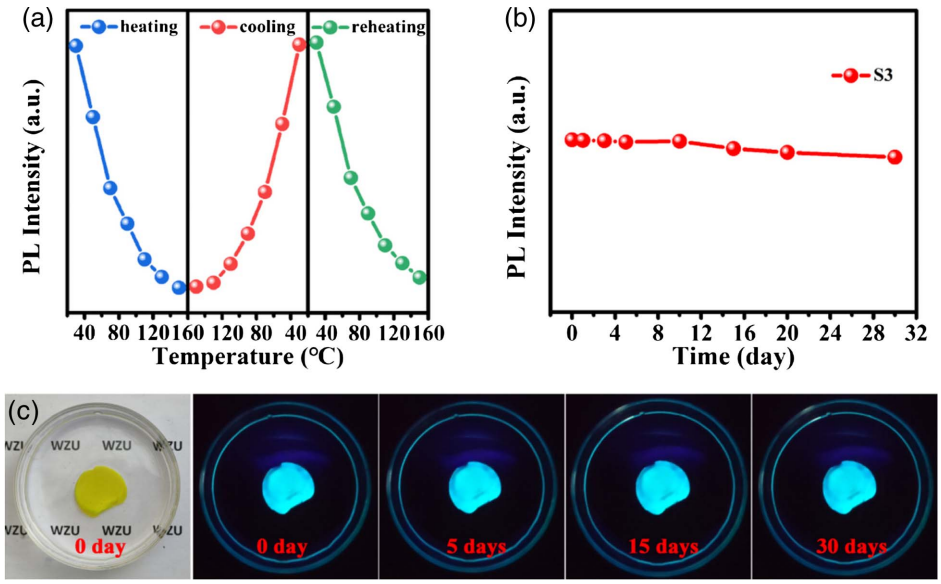

Fig. 4. (a) PL intensity measured during heating, cooling, and reheating. (b) Time-dependent PL intensity. (c) Luminescent photographs of S3 stored in water for different times.

smaller radius. From the perspective of microstructure, it can be clearly seen from the TEM image [Fig. 2(a)] that Gd-doped $CsPbCl_{1.5}Br_{1.5}$ NCs with a circular shape are embedded in the glass matrix. By comparing the high-resolution transmission electron microscope (HRTEM) of doped (S3) and undoped Gd^{3+} (S1), it is concluded that the (1 1 1) lattice fringe spacing of Gd^{3+} doped $CsPbCl_{1.5}Br_{1.5}$ NCs glass is obviously reduced [Figs. 2(b) and 2(c)]. This is the result from partial Gd^{3+} doped into $CsPbCl_{1.5}Br_{1.5}$ NCs glass that causes the crystal lattice to shrink [44]. Figures 2(e)–2(j) show the EDS element distribution of a part of Gd-doped $CsPbCl_{1.5}Br_{1.5}$ NCs glass, which confirms the presence of F, Cl, Br, Cs, Pb, and Gd in Gd-doped $CsPbCl_{1.5}Br_{1.5}$ NCs glass.

The particle size of $CsPbCl_{1.5}Br_{1.5}$ NCs can not only be controlled by metal ions doping, but temperature is also one of the factors that affect the size of the perovskite NCs [45]. Therefore, the different heat treatment temperatures (470°C–10 h, 500°C–10 h, and 530°C–10 h) of Gd-doped $CsPbCl_{1.5}Br_{1.5}$ NCs glasses were explored. As shown in

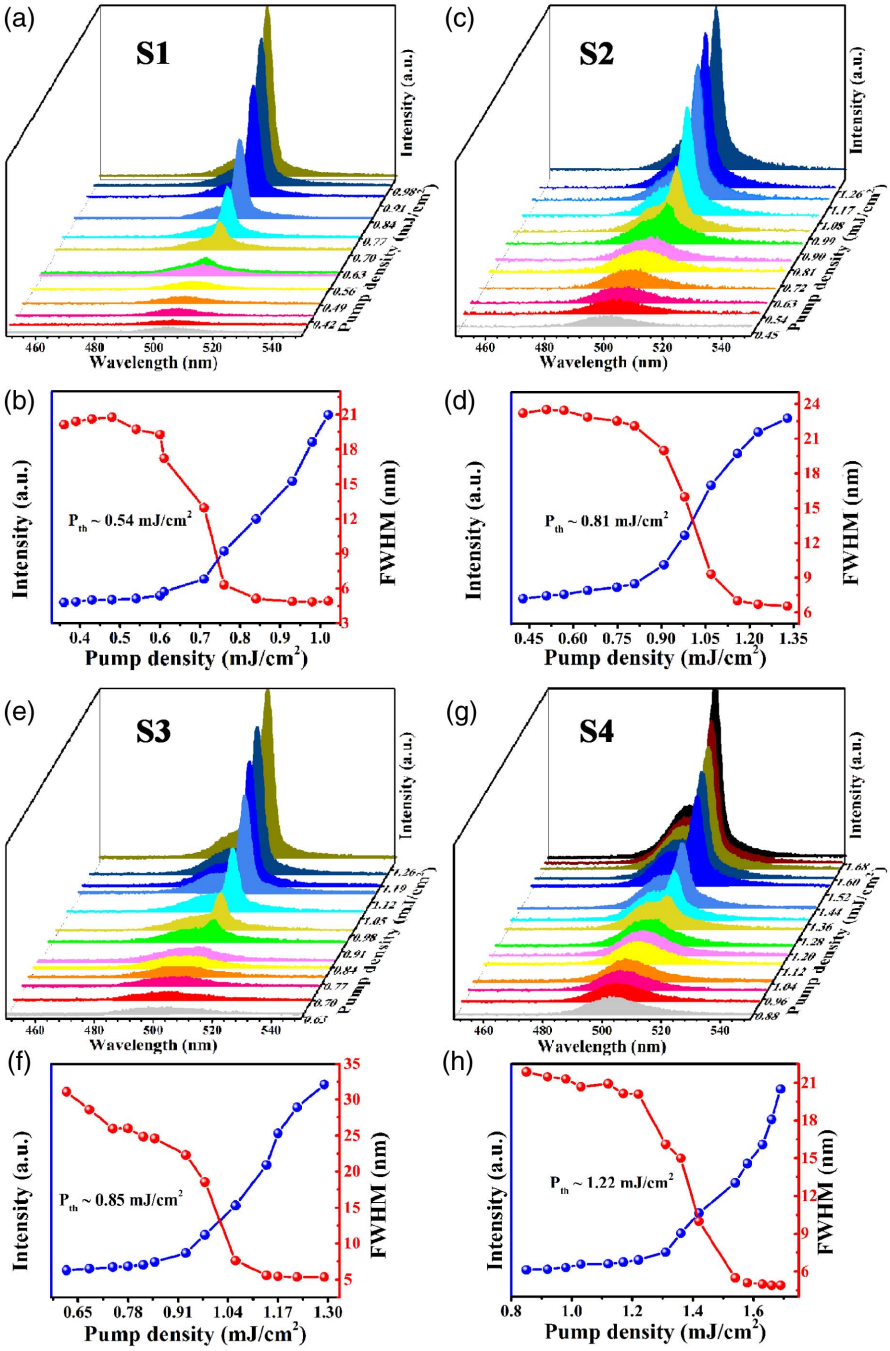

Fig. 5. (a), (c), (e), (g) Pump intensity-dependent PL spectra under increasing 800 nm fs pulsed excitation fluence from the Gd-doped $CsPbCl_{1.5}Br_{1.5}$ NCs glasses (S1–S4). (b), (d), (f), (h) Dependence of the integrated emission intensity (blue lines) and FWHM (red lines) of the emission spectra as a function of pumping density under 800 nm fs laser excitation (S1–S4).

Fig. 3(b), the intensity of PL first increases and then decreases. This is because a proper increase of the heat-treatment temperature is beneficial to the formation and growth of Gd-doped $CsPbCl_{1.5}Br_{1.5}$ NCs, which will cause the intensity of PL to increase. However, the Gd-doped $CsPbCl_{1.5}Br_{1.5}$ NCs become larger when the heat-treatment temperature exceeds the optimal temperature, causing the aggregation of perovskite NCs, which will lead to concentration quenching and weaken the intensity of PL [46]. As the heat-treatment temperature increases from 470°C to 530°C, the intensity of XRD diffraction peaks becomes stronger and tends to shift slightly to a low angle [Fig. 3(a)] for the increase in size of perovskite NCs. The increase in the size of Gd-doped $CsPbCl_{1.5}Br_{1.5}$ NCs will result in a redshift of the PL peak position [Fig. 3(b)] and a decrease in the bandgap [Fig. 3(d)]. In Fig. 3(c), due to the Stokes shift [47], the edge of the absorption spectrum will be located near the PL peak of the corresponding sample. The precise control of the absorption [Fig. 3(c)] and bandgap [Fig. 3(d)] of Gd-doped $CsPbCl_{1.5}Br_{1.5}$ NCs glasses can be successfully achieved by changing the heat treatment temperature.

The quality of the prepared perovskite NCs should be considered, including good optical properties and good stability. Therefore, it is necessary to test the hydrothermal stability of Gd-doped $CsPbCl_{1.5}Br_{1.5}$ NCs glass (S3). The heat resistance of Gd-doped $CsPbCl_{1.5}Br_{1.5}$ NCs glass is pictured in Fig. 4(a). Even after heating, cooling, and reheating, the optical properties of the Gd-doped $CsPbCl_{1.5}Br_{1.5}$ NCs glass can be restored to the original state, showing excellent thermal cycling performance. As shown in Fig. 4(c), the Gd-doped $CsPbCl_{1.5}Br_{1.5}$ NCs glass (S3) was immersed in water, and it can be observed that the S3 remains bright blue light after being stored in water for 30 days without any significant changes, because the borosilicate glass substrate as an ideal protective layer can effectively isolate the Gd-doped $CsPbCl_{1.5}Br_{1.5}$ NCs from the harsh external environment. PL measurements were performed at different times [Fig. 4(b)], and the results show that even after 30 days, the intensity of PL remains around 96%. The above indicates that the Gd-doped $CsPbCl_{1.5}Br_{1.5}$ NCs glass has excellent water resistance. All in all, the prepared Gd-doped $CsPbCl_{1.5}Br_{1.5}$ NCs glass has excellent water/heat resistance.

The laser mechanism of Gd-doped $CsPbCl_{1.5}Br_{1.5}$ NCs glasses is that randomly arranged Gd-doped $CsPbCl_{1.5}Br_{1.5}$ NCs work as both a gain medium and multiple scattering sources. The emitted light undergoes multiple scattering at the grain boundaries and finally returns to the path where they were scattered before, thereby forming a closed-loop cavity. When the optical gain exceeds the loss, laser oscillation is generated at the resonant frequency of the corresponding feedback loop [48]. A series of Gd-doped $CsPbCl_{1.5}Br_{1.5}$ NCs glasses were subjected to 800 nm fs laser experiments at room temperature to explore the relationship between metal ion doping and ASE thresholds. As shown in Figs. 5(a), 5(c), 5(e), and 5(g), when the pump density is lower than the power density that can reach the threshold, the emission spectrum shows a broad emission, namely spontaneous emission (SE), which dominates the PL spectrum of Gd-doped $CsPbCl_{1.5}Br_{1.5}$ NCs glass. But when the pump density exceeds the power density that can achieve the threshold, the sharp increase in the output intensity of Gd-doped $CsPbCl_{1.5}Br_{1.5}$ NCs glass is accompanied by a

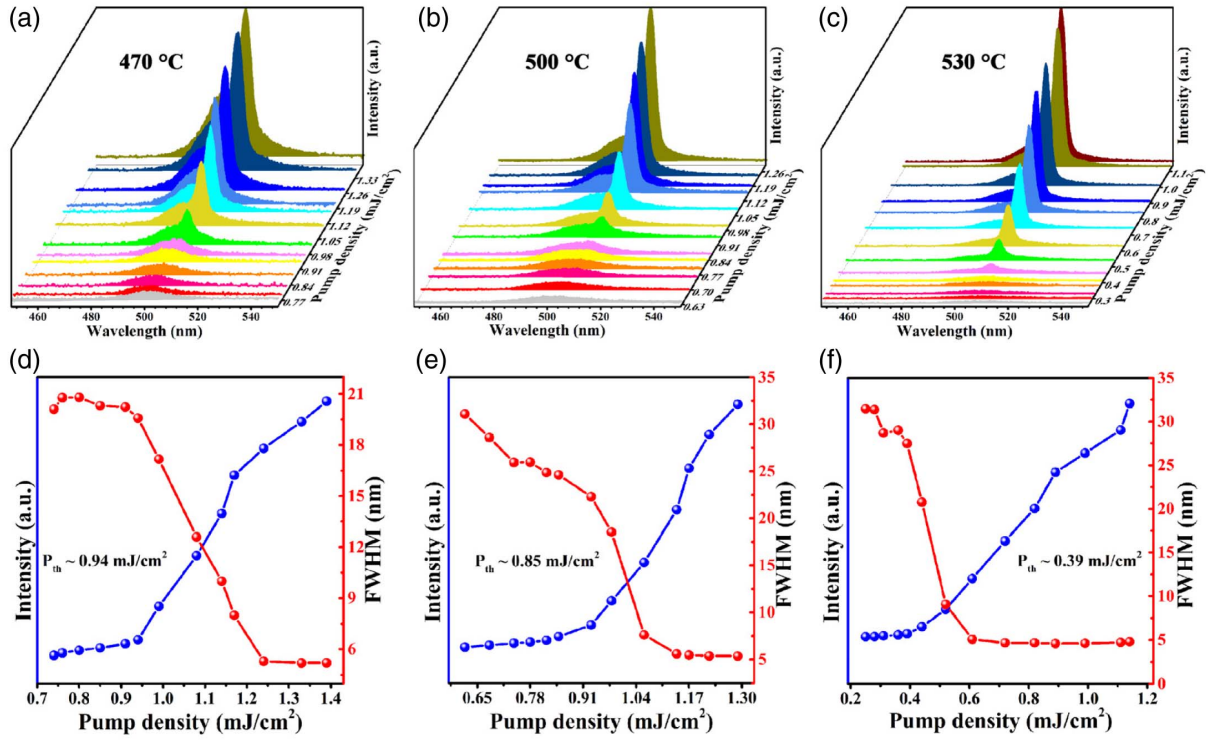

Fig. 6. (a)–(c) Pump intensity-dependent PL spectra under increasing 800 nm fs pulsed excitation fluence from the Gd-doped $CsPbCl_{1.5}Br_{1.5}$ NCs glasses (470°C–530°C). (d)–(f) Dependence of the integrated emission intensity (blue lines) and FWHM (red lines) of the emission spectra as a function of pumping density under 800 nm fs laser excitation (470°C–530°C).

sharp decrease in full width at half-maximum (FWHM), which is the transition from SE to ASE [49]. In the ASE measurement, the blueshift of SE can indeed be attributed to the phase separation of the perovskite NCs. This is because the local electric field destroys the ionic bonds in the mixed halogen NCs [50]. In addition, ASE is located at ~510 nm, which indeed comes from the $CsPbBr_3$-rich phase. In addition, it is found that the ASE peak has a redshift relative to the SE peak, which is caused by the recombination of double excitons [51,52]. Figure 5(b) shows the intensity (blue line) and FWHM (red line) versus pump density. It can be observed that when the pump density exceeds 0.54 mJ/cm^2, the spectra become narrower and the output intensity increases, so $P_{th} = 0.54$ mJ/cm^2 is regarded as the ASE threshold of S1. By analogy, the thresholds of S2–S4 are 0.81 mJ/cm^2, 0.85 mJ/cm^2, and 1.22 mJ/cm^2, respectively [Figs. 5(d), 5(f), and 5(h)]. The gradual increase in the thresholds of Gd-doped $CsPbCl_{1.5}Br_{1.5}$ NCs glasses (S1–S4) is caused by the decrease in the particle size of the perovskite NCs, which also confirms the fact that partial Gd^{3+} ions have been doped into $CsPbCl_{1.5}Br_{1.5}$ NCs.

The effect of Gd-doped $CsPbCl_{1.5}Br_{1.5}$ NCs glasses with different heat treatment temperatures on the ASE thresholds was also researched. As shown in Figs. 6(a)–6(c), the Gd-doped $CsPbCl_{1.5}Br_{1.5}$ NCs glasses with different heat-treatment temperatures have ASE phenomena when the pump density is increased. In addition, the threshold of Gd-doped $CsPbCl_{1.5}Br_{1.5}$ NCs glasses decreases with the increase of heat treatment temperature (470°C–530°C), and the ASE threshold can be as low as 0.39 mJ/cm^2 [Figs. 6(d)–6(f)]. This is the result of the increase in the heat treatment temperature that causes the Gd-doped $CsPbCl_{1.5}Br_{1.5}$ NCs particles to become larger. In short, increasing the heat treatment temperature can obtain Gd-doped $CsPbCl_{1.5}Br_{1.5}$ NCs glass with better crystallinity and larger grain size, making it more suitable for laser applications.

4. CONCLUSION

In summary, a series of Gd-doped $CsPbCl_{1.5}Br_{1.5}$ NCs glasses in borosilicate glass (SiO_2–B_2O_3–ZnO) were successfully prepared. The PL intensity of $CsPbCl_{1.5}Br_{1.5}$ NCs glasses can be improved after doping with Gd^{3+} ions. Specifically, the structure and optical aspect of Gd-doped $CsPbCl_{1.5}Br_{1.5}$ NCs glasses were studied deeply. Furthermore, Gd-doped $CsPbCl_{1.5}Br_{1.5}$ NCs glass shows excellent hydrothermal resistance. It is uplifting that Gd-doped $CsPbCl_{1.5}Br_{1.5}$ NCs glasses can be applied in the ASE field. By studying the effect of different Gd^{3+} doping concentrations and heat treatment temperatures on the $CsPbCl_{1.5}Br_{1.5}$ NCs glasses, it is clarified that the ASE thresholds of perovskite NCs can be adjusted, which lays the foundation for creating more possibilities for the application of perovskite NCs in the laser field in the future.

Funding. National Natural Science Foundation of China (51872207, 52072271).

Disclosures. The authors declare no competing financial interests.

REFERENCES

1. H. Chen, F. Zhou, and Z. Jin, "Interface engineering, the trump-card for $CsPbX_3$ (X = I, Br) perovskite solar cells development," Nano Energy **79**, 105490 (2021).
2. J. Lin, Y. Lu, X. Li, F. Huang, C. Yang, M. Liu, N. Jiang, and D. Chen, "Perovskite quantum dots glasses based backlit displays," ACS Energy Lett. **6**, 519–528 (2021).
3. X. Xiang, H. Lin, J. Xu, Y. Cheng, C. Wang, L. Zhang, and Y. Wang, "$CsPb(Br,I)_3$ embedded glass: fabrication, tunable luminescence, improved stability and wide-color gamut LCD application," Chem. Eng. J. **378**, 122255 (2019).
4. F. Zhou, Z. Li, H. Chen, Q. Wang, L. Ding, and Z. Jin, "Application of perovskite nanocrystals (NCs)/quantum dots (QDs) in solar cells," Nano Energy **73**, 104757 (2020).
5. V. Neplokh, D. I. Markina, M. Baeva, A. M. Pavlov, D. A. Kirilenko, I. S. Mukhin, A. P. Pushkarev, S. V. Makarov, and A. A. Serdobintsev, "Recrystallization of $CsPbBr_3$ nanoparticles in fluoropolymer nonwoven mats for down- and up-conversion of light," Nanomaterials **11**, 412–421 (2021).
6. Y. Zhao, F. Ma, F. Gao, Z. Yin, X. Zhang, and J. You, "Research progress in large-area perovskite solar cells," Photon. Res. **8**, A1–A15 (2020).
7. G. Li, R. Gao, Y. Han, A. Zhai, Y. Liu, Y. Tian, B. Tian, Y. Hao, S. Liu, Y. Wu, and Y. Cui, "High detectivity photodetectors based on perovskite nanowires with suppressed surface defects," Photon. Res. **8**, 1862–1874 (2020).
8. J. Song, J. Li, X. Li, L. Xu, Y. Dong, and H. Zeng, "Quantum dot light-emitting diodes based on inorganic perovskite cesium lead halides ($CsPbX_3$)," Adv. Mater. **27**, 7162–7167 (2015).
9. L. Protesescu, S. Yakunin, M. I. Bodnarchuk, F. Krieg, R. Caputo, C. H. Hendon, R. X. Yang, A. Walsh, and M. V. Kovalenko, "Nanocrystals of cesium lead halide perovskites ($CsPbX_3$, X = Cl, Br, and I): novel optoelectronic materials showing bright emission with wide color Gamut," Nano Lett. **15**, 3692–3696 (2015).
10. M. Lu, J. Guo, S. Sun, P. Lu, X. Zhang, Z. Shi, W. W. Yu, and Y. Zhang, "Surface ligand engineering-assisted $CsPbI_3$ quantum dots enable bright and efficient red light-emitting diodes with a top-emitting structure," Chem. Eng. J. **404**, 126563 (2021).
11. C. Xie, Y. Zhao, W. Shi, and P. Yang, "Postsynthetic surface-treatment of $CsPbX_3$ (X = Cl, Br, or I) nanocrystals via CdX_2 precursor solution toward high photoluminescence quantum yield," Langmuir **37**, 1183–1193 (2021).
12. S. Pan, Y. Chen, Z. Wang, Y.-W. Harn, J. Yu, A. Wang, M. J. Smith, Z. Li, V. V. Tsukruk, J. Peng, and Z. Lin, "Strongly-ligated perovskite quantum dots with precisely controlled dimensions and architectures for white light-emitting diodes," Nano Energy **77**, 105043 (2020).
13. C. Zhang, J. Chen, S. Wang, L. Kong, S. W. Lewis, X. Yang, A. L. Rogach, and G. Jia, "Metal halide perovskite nanorods: shape matters," Adv. Mater. **32**, 2002736 (2020).
14. B. Tang, Y. Hu, J. Lu, H. Dong, N. Mou, X. Gao, H. Wang, X. Jiang, and L. Zhang, "Energy transfer and wavelength tunable lasing of single perovskite alloy nanowire," Nano Energy **71**, 104641 (2020).
15. Y. H. Hsieh, B. W. Hsu, K. N. Peng, K. W. Lee, C. W. Chu, S. W. Chang, H. W. Lin, T. J. Yen, and Y. J. Lu, "Perovskite quantum dot lasing in a gap-plasmon nanocavity with ultralow threshold," ACS Nano **14**, 11670–11676 (2020).
16. D. Xing, C. C. Lin, Y. L. Ho, A. S. A. Kamal, I. T. Wang, C. C. Chen, C. Y. Wen, C. W. Chen, and J. J. Delaunay, "Self-healing lithographic patterning of perovskite nanocrystals for large-area single-mode laser array," Adv. Funct. Mater. **31**, 2006283 (2020).
17. J. M. Pina, D. H. Parmar, G. Bappi, C. Zhou, H. Choubisa, M. Vafaie, A. M. Najarian, K. Bertens, L. K. Sagar, Y. Dong, Y. Gao, S. Hoogland, M. I. Saidaminov, and E. H. Sargent, "Deep-blue perovskite single-mode lasing through efficient vapor-assisted chlorination," Adv. Mater. **33**, 2006697 (2021).
18. Z. He, B. Chen, Y. Hua, Z. Liu, Y. Wei, S. Liu, A. Hu, X. Shen, Y. Zhang, Y. Gao, and J. Liu, "CMOS compatible high-performance nanolasing based on perovskite–SiN hybrid integration," Adv. Opt. Mater. **8**, 2000453 (2020).

19. S. Wang, J. Yu, H. Ye, M. Chi, H. Yang, H. Wang, F. Cao, W. Li, L. Kong, L. Wang, R. Chen, and X. Yang, "Low-threshold amplified spontaneous emission in blue quantum dots enabled by effectively suppressing Auger recombination," Adv. Opt. Mater. **9**, 2100068 (2021).
20. H. Wang, Z. Dong, H. Liu, W. Li, L. Zhu, and H. Chen, "Roles of organic molecules in inorganic $CsPbX_3$ perovskite solar cells," Adv. Energy Mater. **11**, 2002940 (2020).
21. J. Ren, X. Zhou, and Y. Wang, "Dual-emitting $CsPbX_3$@ZJU-28 (X = Cl, Br, I) composites with enhanced stability and unique optical properties for multifunctional applications," Chem. Eng. J. **391**, 123622 (2020).
22. H. Guan, S. Zhao, H. Wang, D. Yan, M. Wang, and Z. Zang, "Room temperature synthesis of stable single silica-coated $CsPbBr_3$ quantum dots combining tunable red emission of Ag–In–Zn–S for high-CRI white light-emitting diodes," Nano Energy **67**, 104279 (2020).
23. F. Li, S. Huang, X. Liu, Z. Bai, Z. Wang, H. Xie, X. Bai, and H. Zhong, "Highly stable and spectrally tunable gamma phase $Rb_xCs_{1-x}PbI_3$ gradient-alloyed quantum dots in PMMA matrix through a sites engineering," Adv. Funct. Mater. **31**, 2008211 (2021).
24. S. Zhao, Q. Mo, W. Cai, H. Wang, and Z. Zang, "Inorganic lead-free cesium copper chlorine nanocrystal for highly efficient and stable warm white light-emitting diodes," Photon. Res. **9**, 1605–1612 (2021).
25. S. Wang, J. Yu, M. Zhang, D. Chen, C. Li, R. Chen, G. Jia, A. L. Rogach, and X. Yang, "Stable, strongly emitting cesium lead bromide perovskite nanorods with high optical gain enabled by an intermediate monomer reservoir synthetic strategy," Nano Lett. **19**, 6315–6322 (2019).
26. L. Protesescu, S. Yakunin, M. I. Bodnarchuk, F. Bertolotti, N. Masciocchi, A. Guagliardi, and M. V. Kovalenko, "Monodisperse formamidinium lead bromide nanocrystals with bright and stable green photoluminescence," J. Am. Chem. Soc. **138**, 14202–14205 (2016).
27. F. Krieg, S. T. Ochsenbein, S. Yakunin, S. T. Brinck, P. Aellen, A. Suess, B. Clerc, D. Guggisberg, O. Nazarenko, Y. Shynkarenko, S. Kumar, C. J. Shih, I. Infante, and M. V. Kovalenko, "Colloidal $CsPbX_3$ (X = Cl, Br, I) nanocrystals 2.0: Zwitterionic capping ligands for improved durability and stability," ACS Energy Lett. **3**, 641–646 (2018).
28. D. Yan, T. Shi, Z. Zang, T. Zhou, Z. Liu, Z. Zhang, J. Du, Y. Leng, and X. Tang, "Ultrastable $CsPbBr_3$ perovskite quantum dot and their enhanced amplified spontaneous emission by surface ligand modification," Small **15**, 1901173 (2019).
29. Y. Luo, T. Tan, S. Wang, R. Pang, L. Jiang, D. Li, J. Feng, H. Zhang, S. Zhang, and C. Li, "Multivariant ligands stabilize anionic solvent-oriented α-$CsPbX_3$ nanocrystals at room temperature," Nanoscale **13**, 4899–4910 (2021).
30. F. Gao, W. Yang, X. Liu, Y. Li, W. Liu, H. Xu, and Y. Liu, "Highly stable and luminescent silica-coated perovskite quantum dots at nanoscale-particle level via nonpolar solvent synthesis," Chem. Eng. J. **407**, 128001 (2021).
31. Q. Zhong, J. Liu, S. Chen, P. Li, J. Chen, W. Guan, Y. Qiu, Y. Xu, M. Cao, and Q. Zhang, "Highly stable $CsPbX_3/PbSO_4$ core/shell nanocrystals synthesized by a simple post-treatment strategy," Adv. Opt. Mater. **9**, 2001763 (2020).
32. W. Lin, G. Chen, E. Li, H. Xie, G. Peng, W. Yu, H. Chen, and T. Guo, "Improved stability and performance of all inorganic perovskite quantum dots synthesized directly with N-alkylmonoamine ligands for light-erasable transistor memory," Org. Electron. **86**, 105869 (2020).
33. W. Xue, X. Wang, W. Wang, F. He, W. Zhu, and Y. Li, "Aluminum distearate–modified $CsPbX_3$ (X = I, Br, or Cl/Br) nanocrystals with enhanced optical and structural stabilities," CCS Chem. **2**, 13–23 (2020).
34. X. Li, C. Yang, Y. Yu, Z. Li, J. Lin, X. Guan, Z. Zheng, and D. Chen, "Dual-modal photon upconverting and downshifting emissions from ultra-stable $CsPbBr_3$ perovskite nanocrystals triggered by co-growth of $Tm:NaYbF_4$ nanocrystals in glass," ACS Appl. Mater. Interfaces **12**, 18705–18714 (2020).
35. T. T. Ngo, I. Suarez, G. Antonicelli, D. Cortizo-Lacalle, J. P. Martinez-Pastor, A. Mateo-Alonso, and I. Mora-Sero, "Enhancement of the performance of perovskite solar cells, LEDs, and optical amplifiers by anti-solvent additive deposition," Adv. Mater. **29**, 1604056 (2017).
36. C. Li, Z. Zang, C. Han, Z. Hu, X. Tang, J. Du, Y. Leng, and K. Sun, "Highly compact $CsPbBr_3$ perovskite thin films decorated by ZnO nanoparticles for enhanced random lasing," Nano Energy **40**, 195–202 (2017).
37. P. K. Roy, G. Haider, H.-I. Lin, Y.-M. Liao, C.-H. Lu, K.-H. Chen, L.-C. Chen, W.-H. Shih, C.-T. Liang, and Y.-F. Chen, "Multicolor ultralow-threshold random laser assisted by vertical-graphene network," Adv. Opt. Mater. **6**, 1800382 (2018).
38. N. Pourdavoud, T. Haeger, A. Mayer, P. J. Cegielski, A. L. Giesecke, R. Heiderhoff, S. Olthof, S. Zaefferer, I. Shutsko, A. Henkel, D. Becker-Koch, M. Stein, M. Cehovski, O. Charfi, H. H. Johannes, D. Rogalla, M. C. Lemme, M. Koch, Y. Vaynzof, K. Meerholz, W. Kowalsky, H. C. Scheer, P. Gorrn, and T. Riedl, "Room-temperature stimulated emission and lasing in recrystallized cesium lead bromide perovskite thin films," Adv. Mater. **31**, 1903717 (2019).
39. M. Jin, S. Huang, C. Quan, X. Liang, J. Du, Z. Liu, Z. Zhang, and W. Xiang, "Blue low-threshold room-temperature stimulated emission from thermostable perovskite nanocrystals glasses through controlling crystallization," J. Eur. Ceram. Soc. **41**, 1579–1585 (2021).
40. Z. Zhang, L. Shen, H. Zhang, L. Ding, G. Shao, X. Liang, and W. Xiang, "Novel red-emitting $CsPb_{1-x}Ti_xI_3$ perovskite QDs@glasses with ambient stability for high efficiency white LEDs and plant growth LEDs," Chem. Eng. J. **378**, 122125 (2019).
41. C. M. Guvenc, Y. Yalcinkaya, S. Ozen, H. Sahin, and M. M. Demir, "Gd^{3+}-doped α-$CsPbI_3$ nanocrystals with better phase stability and optical properties," J. Phys. Chem. C **123**, 24865–24872 (2019).
42. D. Chen, Y. Liu, C. Yang, J. Zhong, S. Zhou, J. Chen, and H. Huang, "Promoting photoluminescence quantum yields of glass-stabilized $CsPbX_3$ (X = Cl, Br, I) perovskite quantum dots through fluorine doping," Nanoscale **11**, 17216–17221 (2019).
43. E. Cao, J. Qiu, D. Zhou, Y. Yang, Q. Wang, and Y. Wen, "The synthesis of a perovskite $CsPbBr_3$ quantum dot superlattice in borosilicate glass," Chem. Commun. **56**, 4460–4463 (2020).
44. G. Shao, S. Liu, L. Ding, Z. Zhang, W. Xiang, and X. Liang, "$K_xCs_{1-x}PbBr_3$ NCs glasses possessing super optical properties and stability for white light emitting diodes," Chem. Eng. J. **375**, 122031 (2019).
45. X. Liu, E. Mei, Z. Liu, J. Du, X. Liang, and W. Xiang, "Stable, low-threshold amplification spontaneous emission of blue-emitting $CsPbCl_2Br_1$ perovskite nanocrystals glasses with controlled crystallization," ACS Photonics **8**, 887–893 (2021).
46. Y. Zhang, J. Liu, H. Zhang, Q. He, X. Liang, and W. Xiang, "Ultra-stable Tb^{3+}: $CsPbI_3$ nanocrystal glasses for wide-range high-sensitivity optical temperature sensing," J. Eur. Ceram. Soc. **40**, 6023–6030 (2020).
47. L. Zhang, F. Yuan, H. Dong, B. Jiao, W. Zhang, X. Hou, S. Wang, Q. Gong, and Z. Wu, "One-step co-evaporation of all-inorganic perovskite thin films with room-temperature ultralow amplified spontaneous emission threshold and air stability," ACS Appl. Mater. Interfaces **10**, 40661–40671 (2018).
48. M. L. De Giorgi and M. Anni, "Amplified spontaneous emission and lasing in lead halide perovskites: state of the art and perspectives," Appl. Sci. **9**, 4591 (2019).
49. D. Vila-Liarte, M. W. Feil, A. Manzi, J. L. Garcia-Pomar, H. Huang, M. Doblinger, L. M. Liz-Marzan, J. Feldmann, L. Polavarapu, and A. Mihi, "Templated-assembly of $CsPbBr_3$ perovskite nanocrystals into 2D photonic supercrystals with amplified spontaneous emission," Angew. Chem. **59**, 17750–17756 (2020).
50. H. Zhang, X. Fu, Y. Tang, H. Wang, C. Zhang, W. W. Yu, X. Wang, Y. Zhang, and M. Xiao, "Phase segregation due to ion migration in all-inorganic mixed-halide perovskite nanocrystals," Nat. Commun. **10**, 1088 (2019).
51. Y. Wang, X. Li, J. Song, L. Xiao, H. Zeng, and H. Sun, "All-inorganic colloidal perovskite quantum dots: a new class of lasing materials with favorable characteristics," Adv. Mater. **27**, 7101–7108 (2015).
52. S. Li, D. Lei, W. Ren, X. Guo, S. Wu, Y. Zhu, A. L. Rogach, M. Chhowalla, and A. K. Jen, "Water-resistant perovskite nanodots enable robust two-photon lasing in aqueous environment," Nat. Commun. **11**, 1192 (2020).